

Original Article
Biomedical Engineering



OPEN ACCESS

Received: Sep 5, 2019

Accepted: Sep 19, 2019

Address for Correspondence:

In-Kyu Park, PhD

Department of Biomedical Science and BK21 PLUS Centre for Creative Biomedical Scientists, Chonnam National University Medical School, 160 Baekseo-ro, Dong-gu, Gwangju 61469, Republic of Korea.
E-mail: pik96@chonnam.ac.kr

Woo Kyun Bae, MD, PhD

Department of Hematology-Oncology, Chonnam National University Medical School and Hwasun Hospital, 264 Seoyang-ro, Hwasun 58128, Republic of Korea.
E-mail: drwookyun@chonnam.ac.kr

© 2019 The Korean Academy of Medical Sciences.

This is an Open Access article distributed under the terms of the Creative Commons Attribution Non-Commercial License (<https://creativecommons.org/licenses/by-nc/4.0/>) which permits unrestricted non-commercial use, distribution, and reproduction in any medium, provided the original work is properly cited.

ORCID iDs

Kondareddy Cherukula <https://orcid.org/0000-0003-4205-1634>

Myung Suk Park <https://orcid.org/0000-0002-3653-1546>

Adonijah Graham Sontyana <https://orcid.org/0000-0002-8904-7694>

Ansuja Pulickal Mathew <https://orcid.org/0000-0001-5025-1623>

Veena Vijayan <https://orcid.org/0000-0001-8072-2406>

Role of Immunosuppressive Microenvironment in Acquiring Immunotolerance Post-Photothermal Therapy

Kondareddy Cherukula ¹, Myung Suk Park ², Adonijah Graham Sontyana ¹, Ansuja Pulickal Mathew ¹, Veena Vijayan ¹, Woo Kyun Bae ² and In-Kyu Park ¹

¹Department of Biomedical Science and BK21 PLUS Centre for Creative Biomedical Scientists, Chonnam National University Medical School, Gwangju, Korea

²Department of Hematology-Oncology, Chonnam National University Medical School and Hwasun Hospital, Hwasun, Korea

ABSTRACT

Background: Nanoparticle-mediated photothermal therapy (PTT) has been well studied as a treatment for cancer. However, the therapeutic outcome of PTT is often hindered by the penetration depth of laser light. In the tumor margin beyond the laser penetration limit, tumor recurrence often occurs, bypassing the immune response of the host. Accumulating evidence suggests the prominent role of tumor microenvironment (TME) and its interactions with the immune components contribute to an immunosuppressive milieu during the post-therapy period. Here, we explored the immunosuppressive cascade generated after PTT, which is responsible for tumor recurrence, and identified the potential targets to achieve an effective PTT period.

Methods: Here, we investigated the immunosuppressive cascade generated after PTT in a CT26 tumor bearing mouse. The liposomal system loaded with the indocyanine green (ICG) was utilized for the generation of PTT with high efficiency. Immunological factors such as cytokines and protein expressions post-therapy were investigated through enzyme-linked immunosorbent assay, flow cytometry and western blot analysis.

Results: Our results suggested that PTT with ICG-loaded liposomes (Lipo-ICG) was effective for the first 5 days after treatment, resulting in tumor suppression. However, an immunosuppressive and pro-inflammatory environment developed thereafter, causing the recruitment and upregulation of the immune evasion factors of heat shock protein 70, programmed death ligand 1, indoleamine-dioxygenase, interleukin-6, transforming growth factor- β , regulatory T-cells, and myeloid-derived suppressor cells, to develop immunotolerance.

Conclusion: Collectively, these findings have determined potential therapeutic targets to modulate the TME during PTT and achieve tumor ablation without remission.

Keywords: Photothermal Therapy; Immunosuppression; Tumor Microenvironment; Immunosuppression

Woo Kyun Bae <https://orcid.org/0000-0003-0267-1943>In-Kyu Park <https://orcid.org/0000-0003-1616-9153>**Funding**

This work was financially supported by Basic Science Research Program (No. 2016R1A2B4011184) and the Bio & Medical Technology Development Program (No. NRF-2017M3A9F5030940, NRF-2017M3A9E2056372 and NRF-2017M3A9E2056374) through the National Research Foundation of Korea (NRF) funded by the Korean government, MSIP. This work was supported by the National Research Foundation of Korea (NRF) grant funded by the Korea government (MSIT) (No. 2018R1A5A2024181).

Disclosure

The authors have no potential conflict of interest to disclose.

Author Contributions

Conceptualization: Bae WK, Park IK. Formal analysis: Cherukula K, Park MS. Investigation: Cherukula K, Park MS, Mathew AP, Vijayan V, Sontyana AG. Methodology: Cherukula K, Park MS, Sontyana AG. Writing - original draft: Cherukula K, Park MS. Writing - review & editing: Cherukula K, Park MS, Bae WK, Park IK. Supervision: Bae WK, Park IK.

INTRODUCTION

The antitumor responses to cancer therapies are transitory and often result in tumor recurrence. Despite numerous efficient strategies to kill the tumor cells, it is difficult to eradicate all the residual tumor cells owing to their temporal and spatial tumor variability, and tumor cell resistance, which often results in tumor recurrence.¹ Although the surgical resection of primary tumors improves the survival period of patients, undetected small regions of the tumor may develop into major regions of aggressive cancer, such as cancers of the colon and the lung.² This type of cancer recurrence is mainly promoted by the highly suppressive tumor microenvironment. Clinical studies suggest that conventional treatment modalities, such as radiation therapy, have been shown to promote an immunosuppressive environment, including the generation of pro-tumorigenic M2 macrophages, regulatory T cells (T_{regs}), and transforming growth factor β (TGF- β).³ Despite the effectiveness of antitumor responses, the immunosuppressive microenvironment that develops post radiation therapy hampers the effectiveness of radiation therapies. Thus, there is an urgent need to combine the immunotherapy strategies with conventional treatments to improve the antitumor therapeutic efficacy.

Recently, photothermal therapy (PTT) has attracted much attention owing to its effective therapeutic index. In PTT, near infrared (NIR) light-absorbing materials accumulated specifically in the tumor region are heated up by an externally applied NIR laser exert irreversible damage to the tumor tissue.⁴ However, although tumor cells undergo irreversible cell damage when exposed to hyperthermic stress post PTT, they often release pro-inflammatory components.⁵ These pro-inflammatory responses may enhance the conventional therapies, such as chemotherapy, through immune-mediated tumor eradication.⁶ However, therapy-associated chronic inflammation promotes immunosuppression characterized by the infiltration of pro-inflammatory mediators, immune suppressor cells, and checkpoint pathways inhibiting the T cell responses.⁷ This further aggravates tumor progression, tumor-associated trauma, and tumor resistance to anticancer therapies.^{6,8} In addition, evidence has accumulated to suggest that, globally, 20% of cancers are associated with chronic inflammation.⁹

The tumor microenvironment (TME) is characterized by a broad variety of signaling cascades; as a result, various immune cells are activated by their interaction with the host. Tumor cells in the TME try to circumvent immune system-mediated recognition. In addition, tumor cells in the TME divert the immune responses through the induction of the immunoregulatory factors that will promote the disease progression.^{10,11} The major drawbacks with the conventional therapies, such as radiation therapy, are associated with excessive tissue damage and accompanied by the onset of inflammatory cytokines, which cause further progression of tumor development.¹² Very few studies have investigated PTT-associated inflammation and the subsequent tumor regression through the utilization of anti-inflammatory drugs⁷ and metabolic inhibitors.¹² However, a comprehensive research about the tumor microenvironmental changes that dictate the tumor growth post PTT has not been reported yet.

Liposomes are utilized widely in the design of drug delivery systems, which can target the tumor via the enhanced permeation and retention (EPR) effect.¹³ In addition, liposomes can be engineered as theranostic vehicles through the accommodation of both therapeutic and imaging agents.¹⁴ Indocyanine green (ICG), an FDA-approved NIR dye, has been

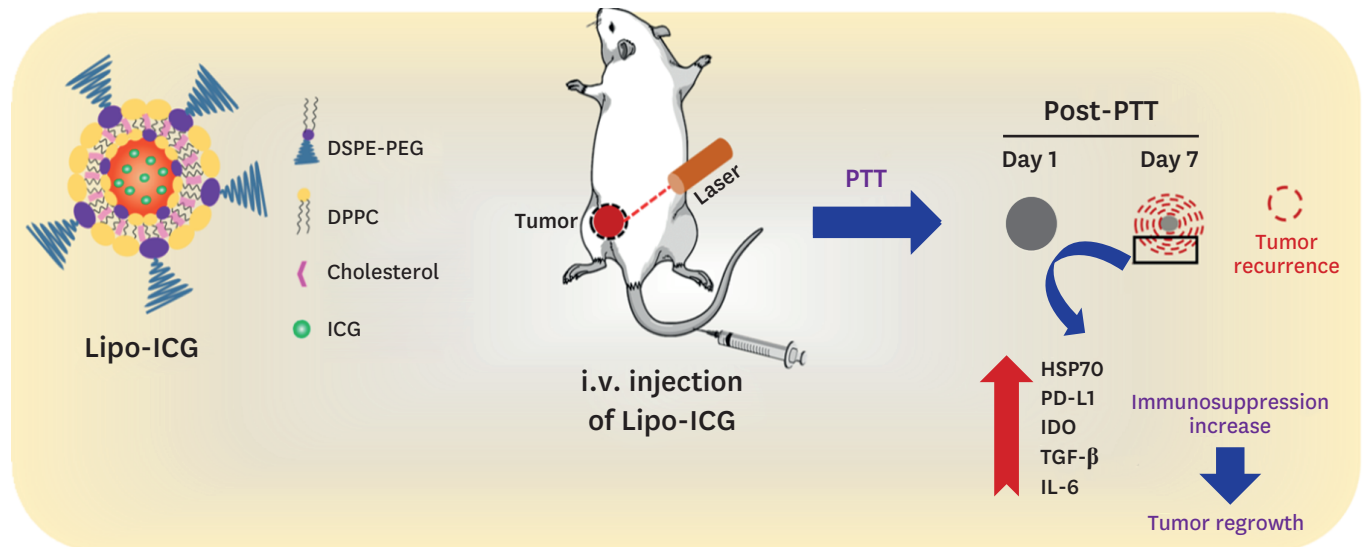


Fig. 1. Schematic illustration of Lipo-ICG composition and the application of Lipo-ICG as a tumor ablating agent. When the tumor is treated with PTT, effective PTT only occurs in tumor tissue several millimeters deep. The remaining tumor tissue (tumor margin) undergoes ineffective PTT, in which HSP, IDO, TGF- β , PD-L1, and IL-6 are upregulated, which accelerated tumor recurrence.

Lipo-ICG = indocyanine green-loaded liposomes, DSPE-PEG = 1,2-distearoyl-sn-glycero-3-phosphoethanolamine-N-[methoxy(polyethylene glycol)-2000], DPPC = dipalmitoyl-sn-glycero-3-phosphocholine, ICG = indocyanine green, PTT = photothermal therapy, HSP = heat shock protein, PD-L1 = programmed death ligand 1, IDO = indoleamine dioxygenase, TGF- β = tumor growth factor- β , IL-6 = interleukin-6.

explored extensively in many PTT studies,^{15,16} and was therefore chosen as a representative PTT agent for this study. We utilized 1,2-distearoyl-sn-glycero-3-phosphoethanolamine-N-[methoxy(polyethylene glycol)-2000] (DSPE-PEG) and dipalmitoyl-sn-glycero-3-phosphocholine (DPPC) within a liposomal formulation to fabricate a stable and neutrally charged liposome, with enhanced circulation and tumor-targeting properties.

In this study, we synthesized ICG-loaded liposomes (Lipo-ICG) to investigate the immunosuppressive factors expressed and secreted in the tumor region after PTT (Fig. 1). ICG could be effectively loaded into liposomes to induce tumor ablation in the tumor region, and immunosuppressive molecules and modulators were assessed in peripheral blood, splenocytes, and the tumor at different time points after PTT. Furthermore, this work identifies new attractive targets to enhance the therapeutic efficacy, overcome the immunosuppressive cascade, and result in significant cancer therapy.

METHODS

Materials

1,2-Distearoyl-sn-glycero-3-phosphoethanolamine-N-[methoxy(polyethylene glycol)-2000] (DSPE-PEG), cholesterol, and dipalmitoyl-sn-glycero-3-phosphocholine (DPPC) were purchased from Avanti Polar Lipids (Alabaster, AL, USA). ICG was purchased from BioActs (Seoul, Korea). 3-(4,5-Dimethylthiazol-2-yl)-5-(3-carboxymethoxyphenyl)-2-(4-sulfophenyl)-tetrazolium (MTS) reagent was obtained from Promega (Madison, WI, USA). Dulbecco's modified Eagle's medium (DMEM) and Ellman's reagent were obtained from Thermo Scientific (Waltham, MA, USA). All other chemicals were obtained from commercial suppliers, unless otherwise specified.

Synthesis of liposomes and liposome-ICG

Liposomes were synthesized by using a thin film hydration method,¹⁷ and then extruded. Briefly, DPPC, DSPE-PEG, and cholesterol lipids in a 1.5:1.5:1 (wt. ratio) were mixed in chloroform and then a lipid film was formed by the evaporation of chloroform. Next, the lipid film was hydrated for 30 minutes at 60°C by the addition of PBS solution, which produced heterogeneous and multivesicular liposomes. The obtained solution was passed through a 200 nm polycarbonate filter and fixed by using an Avanti Mini-Extruder (Avanti Polar Lipids) to obtain liposomes. ICG was loaded into liposomes during the hydration process. An aqueous solution containing ICG was added to liposomes at weight ratio of 1:100 and hydrated for 30 minutes at 60°C, then extruded through a 200 nm polycarbonate filter mounted in an Avanti Mini-Extruder. Excess ICG solution was removed by using 100 kDa centrifugal filters (Merck Millipore Co., Dublin, Ireland).

Characterization of nanoparticles (NPs)

The NP size and zeta potential were assessed by dynamic light scattering (DLS) using a Zetasizer Nano Z (Malvern Instruments, Malvern, UK). The morphology of NPs was analyzed by using a field emission transmission electron microscope (FE-TEM) (JEM-2100F, Peabody, MA, USA). UV absorbance was analyzed by using a UV-VIS spectrophotometer (UV-2700, Shimadzu, Columbia, MD, USA). The thermal elevations of ICG (30 µg/mL) and Lipo-ICG (30 µg/mL ICG) and thermal images were captured and analyzed by thermal camera (Avio IR camera/Thermometer, Tokyo, Japan).

Biodistribution and photothermal therapy

Four-week-old BALB/c female mice were injected in the right flank with 1×10^6 CT-26 cells and biodistribution studies were conducted when the tumors reached 100 mm³. Lipo-ICG, equivalent to an ICG dosage of 1 mg/kg, was injected intravenously and tracked by using a fluorescence-labeled organism bio-imaging instrument (FOBI, NEO Science, Seoul, Korea). The 808 nm laser was irradiated by a power intensity of 2 W/cm² onto tumors for 10 minutes, and tumor temperature was recorded by using a thermal camera (Avio IR camera/Thermometer). The tumor volume and mouse weight were recorded for 15 days after treatment.

Flow cytometry analysis

For the analysis of circulating immune cells after PTT treatment, red blood cells were removed in ACK lysis buffer, and splenocytes and PBMCs were collected. The cell suspensions were filtered through a 70 µm strainer and washed with FACS buffer (1% BSA in PBS); the cells were then stained with fluorescence-labeled antibodies purchased from eBioscience (San Diego, CA, USA). CD3⁺CD4⁺CD8a⁺, CD3⁺CD4⁺CD8a⁻, CD3⁺CD4⁺Foxp3⁺, and CD3⁺CD8a⁺IFN-γ⁺ cell populations were identified by using the following surface markers: CD3-FITC Rat anti-mouse, anti-CD8a-PerCP, anti-IFN-γ-APC, and anti-CD279-PE. T_{regs} were evaluated by using anti-CD4-APC, anti-CD25-FITC, and anti-Foxp3-PE antibodies in accordance with the manufacturer's protocols. Myeloid-derived suppression cells were determined by labeling with anti-CD11b-FITC and anti-Gr-1-APC•Cy7. In the flow cytometric analyses, all antibodies were used at 1:100 dilutions. The labeled cells were analyzed by using a FACS Canto II Cell analyzer and the data were further processed by using FACSDiva software (BD Bioscience, San Jose, CA, USA).

Cytokine detection

Serum samples were isolated from mice after various treatments and diluted for analysis. TGF-β1 (R&D Systems, Minneapolis, MN, USA) was analyzed by using enzyme-linked

immunosorbent assay (ELISA) kits in accordance with R&D Systems protocols. The plates were read at an optical density (O.D.) at 450 nm by using an ELISA reader system.

Western blotting analysis

Briefly, the tumor tissues of each group were lysed on ice in T-PER Tissue Protein Extraction Reagent (Thermo Scientific, Waltham, MA, USA) containing protease and phosphatase inhibitors cocktails (Thermo Scientific), and centrifuged to obtain the protein supernatant. Subsequently, the total protein concentration was measured by using the BCA assay (Thermo Scientific) and 30 μ g of each protein was loaded on an SDS-PAGE gel. After the proteins were separated, the resulting gels were transferred to PVDF membranes (Millipore, Burlington, CA, USA). Non-specific binding to the gel was blocked by using Super Block T20 blocking buffer (Thermo Scientific) diluted in PBS. Rabbit monoclonal antibodies against PD-L1 (Cell Signaling Technology, Danvers, MA, USA) and β -actin (Abcam, Cambridge, MA, USA); mouse monoclonal antibodies against HSP70 and IL-6 (Santa Cruz Biotechnology, Dallas, TX, USA); and rat monoclonal antibody against IDO (Santa Cruz Biotechnology) were employed for western blotting analysis. The primary antibodies were incubated with the PVDF membrane overnight at 4°C with shaking, washed, and then incubated with the corresponding HRP-conjugated secondary antibodies (Jackson Immuno Research Laboratories, West Grove, PA, USA) for 1 hour at room temperature. Then, blots were washed three times for 20 minutes with TBST buffer to remove any residual primary and secondary antibodies. The blots were pre-incubated with Immobilon Forte Western HRP Substrate (Millipore, Bedford, MA, USA) and protein signals were measured by using a luminescent image analyzer (LAS-4000 mini, Fujifilm, Tokyo, Japan). Band quantification was performed by using multi-gauge software (Fujifilm).

Statistical analysis

All the data represented as mean \pm standard deviation. Statistical analysis was analyzed by Student's *t*-test.

Ethics statement

Experiments on animals were approved by the Ethics Committee of Chonnam National University Medical School and Chonnam National University Hwasun Hospital, Korea (CNU IACUC-H-2018-59).

RESULTS

Liposome synthesis and characterization

Liposomes were synthesized by using a thin film hydration method with the lipid components of DPPC, cholesterol, and DSPE-PEG at weight ratio of 1.5:1.5:1 and then loaded with ICG (Fig. 2A). The liposomes synthesized by the extrusion method were characterized by using an FE-TEM. The diameter of the liposomes was observed to be 107 nm and 93 nm before and after ICG loading, respectively (Fig. 2B and C). Similarly, DLS analyses of liposomes and Lipo-ICG were performed (Fig. 2D and Supplementary Table 1). The hydrodynamic size of the liposomes and Lipo-ICG was 120 ± 4 nm and 122 ± 6 nm, respectively, and a slightly negative zeta potential was observed, of -4 ± 1.4 mV and -8.9 ± 2.3 mV, respectively, for the liposomes and Lipo-ICG. In addition, ICG insertion into the liposomes was confirmed by UV-VIS, with a characteristic peak at 778 nm (Fig. 2E). The as-prepared liposomes and Lipo-ICG were stable, without any precipitation (Fig. 2G). Thermal images of ICG and Lipo-ICG showed

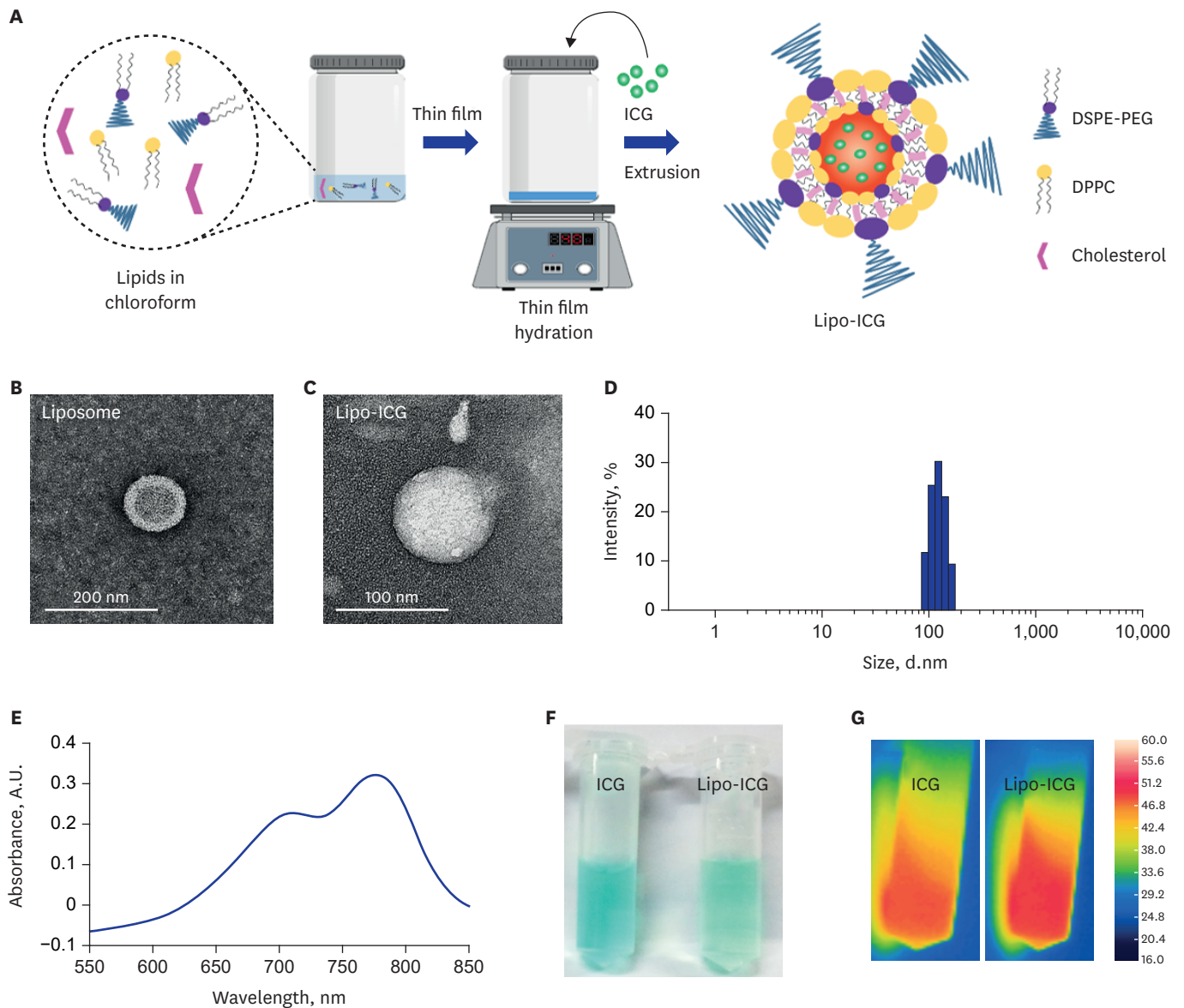


Fig. 2. Characterization of Lipo-ICG. (A) Scheme of Lipo-ICG synthesis. FE-TEM images of (B) liposome and (C) Lipo-ICG. (D) UV-VIS spectrum of Lipo-ICG. (E) Digital photographs of ICG and Lipo-ICG. (F) Thermal images of ICG and Lipo-ICG recorded after 808 nm laser irradiation for 15 minutes at 2 W/cm². (G) DLS profile of Lipo-ICG. ICG = indocyanine green, Lipo-ICG = indocyanine green-loaded liposomes, DSPE-PEG = 1,2-distearoyl-sn-glycero-3-phosphoethanolamine-N-[methoxy(polyethylene glycol)-2000], DPPC = dipalmitoyl-sn-glycero-3-phosphocholine, FE-TEM = field emission transmission electron microscope, DLS = dynamic light scattering.

hyperthermia, with temperatures reaching 48°C and 52°C, respectively, after 5 minutes of irradiation with an 808 nm laser (Fig. 2G and Supplementary Fig. 1).

Biodistribution and in vivo thermal elevation

Lipo-ICG (1 mg/kg ICG) was injected intravenously to CT26 tumor-bearing mice, and tumor targeting was tracked via in vivo fluorescence imaging. As shown in Fig. 3A, Lipo-ICG accumulation in the tumor region (black dotted circle) was increased during the first 12 hours post-administration, and decreased thereafter, with concomitantly rapid clearing from other organs. As the tumor targeting of the Lipo-ICG NPs was promising, we then investigated the thermal enhancement upon laser irradiation in the tumor region. At 24 hours after Lipo-ICG administration, CT26 tumor-bearing mice were irradiated. The thermal images were

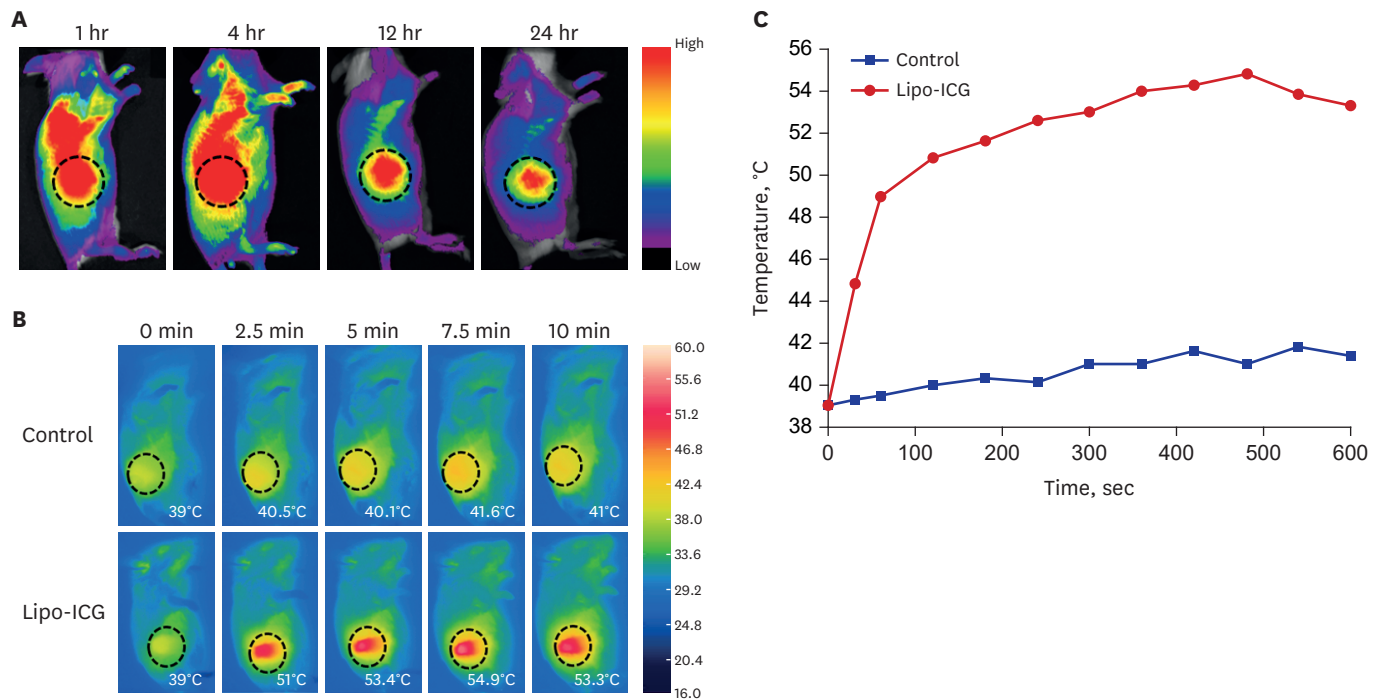


Fig. 3. Biodistribution and in vivo PTT efficacy of Lipo-ICG. **(A)** In vivo fluorescence images for the first 24 hours after Lipo-ICG were injected intravenously to tumor-bearing mice. **(B)** Thermal images of CT26 tumor-bearing mice after an intravenous injection of Lipo-ICG (1 mg/kg ICG) or PBS, followed by laser irradiation (808 nm, 2 W/cm², 10 minutes). **(C)** Temperature changes observed in tumor during the irradiation period. Lipo-ICG = indocyanine green-loaded liposomes, PTT = photothermal therapy, ICG = indocyanine green.

captured and the temperature changes in the tumor were recorded for the irradiation period. As shown in **Fig. 3B and C**, the tumor temperature of Lipo-ICG-treated group increased from the normal surface temperature of the body to approximately 53°C, whereas the PBS-treated group did not exhibit appreciable thermal elevation.

Photothermal therapy accelerated tumor recurrence in the tumor margin

Then, we investigated the tumor regression ability of Lipo-ICG and PTT efficacy was measured as a means of tumor volume reduction. After the administration of Lipo-ICG at a dosage of 1 mg/kg ICG for 24 hours and 808 nm laser irradiation at 2 W/cm² for 10 minutes, tumor regression was observed, characterized by the reduction in tumor volumes for 7–8 days post-treatment (**Fig. 4A and B**). However, the tumor volume started to increase after 8 days of treatment, and increased rapidly for the 15 days of the observation period. All mice survived over an observation period of up to 15 days without any significant fluctuations in their body weight (**Fig. 4C**). This result also indicated that PTT became ineffective after 7 days. Therefore, we were encouraged to identify the changes in the TME after laser irradiation to determine potential therapeutic targets and efficient therapeutic devices.

Immunotolerance evaluation after PTT

We hypothesized that immunotolerance that develops after PTT is the main cause for tumor regrowth, as shown in **Fig. 4B**. We evaluated the immune responses in the spleen and peripheral blood to determine the changes in the immune response induced by PTT. Flow cytometry of the spleen on Day 2 and Day 5 after PTT was analyzed and quantified (**Fig. 5A and Supplementary Table 2**). As shown in **Fig. 5A**, there were no significant changes in the tested immunological factors between the control- and PTT-treated samples on Day 2 and Day

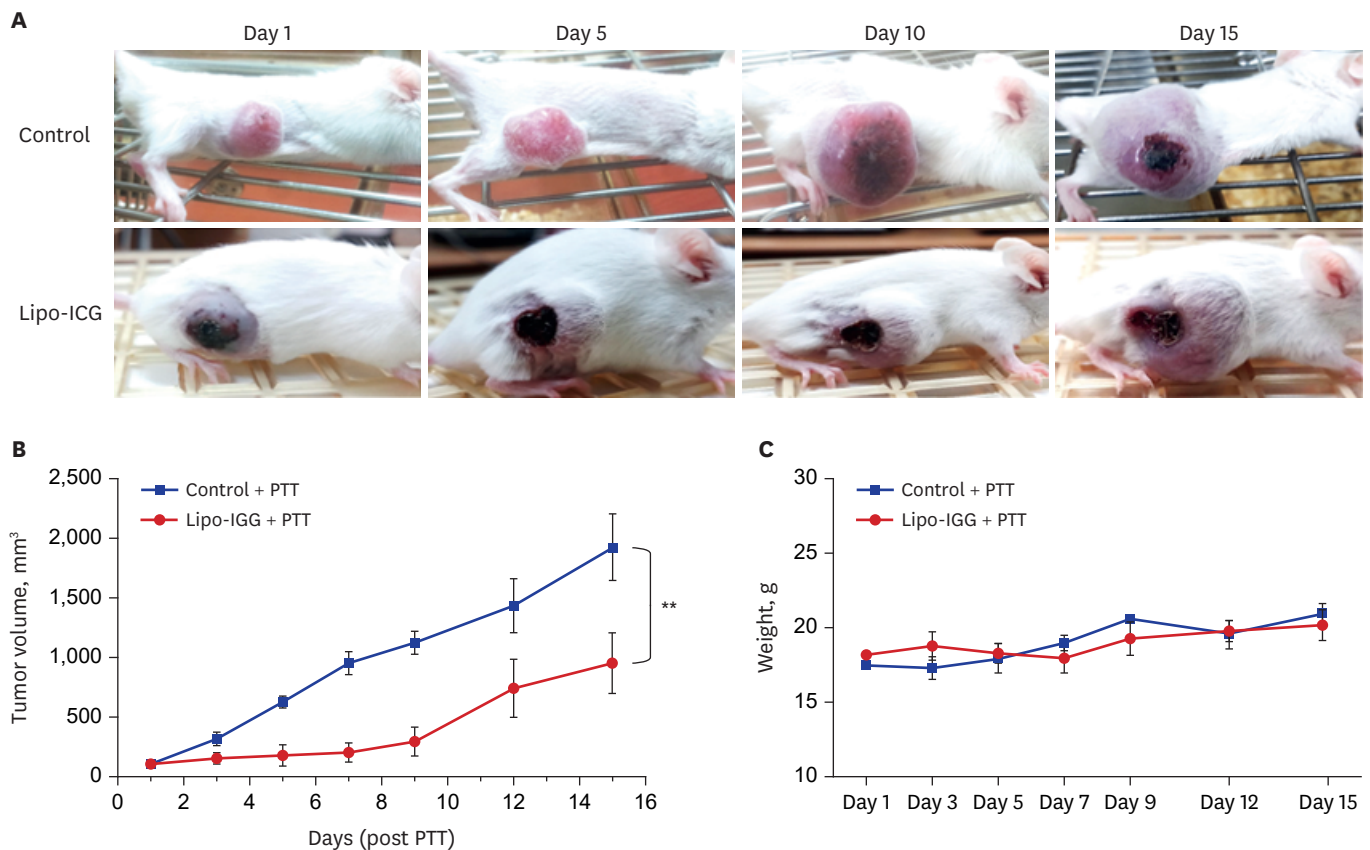


Fig. 4. Anti-tumor efficacy of Lipo-ICG in CT26 tumor bearing mice. **(A)** Representative images of CT26 tumor-bearing mice after photothermal treatment. **(B)** Tumor volume changes in treated mice. **(C)** Mouse body weight changes over the treatment period. Statistical significance was calculated by Student's *t*-test and indicated by ** $P < 0.01$.

PTT = photothermal therapy, Lipo-ICG = indocyanine green-loaded liposomes.

5 after PTT. In contrast, the percentage of whole T cells (CD3⁺) in the PTT-treated group was significantly increased on Day 10 and Day 15 compared with the control group, as shown in Fig. 5B. In addition, CD4⁺CD25⁺Foxp3⁺ population was significantly higher at Day 10 after PTT compared with the control. In addition, a modest increase in the levels CD11b⁺PD-L1⁺ in the PTT-treated group was also observed on Day 10 and Day 15 compared with the control group.

Similarly, peripheral blood was analyzed to investigate the immune suppression factors on Day 2 and Day 5 post PTT (Fig. 6A and Supplementary Table 3). The results indicated that there were no significant changes between the control- and PTT-treated groups up to Day 5. In contrast, the percentage of CD3⁺ whole T cells was significantly lower than the control in PTT-treated samples. As shown in Fig. 6B, the percentage of CD3⁺CD4⁺PD-1⁺ cells were enhanced in the PTT-treated group from Day 10 onwards and led to a significant increase on Day 15. Similarly, the percentage of CD3⁺CD8a⁺IFN- γ ⁺ cells was enhanced on Day 10 and Day 15 compared with the controls, which indicated the special role of IFN- γ in disease progression.¹⁸ In addition, we observed a moderate rise in CD4⁺CD25⁺Foxp3⁺ levels in the PTT-treated group compared with the control group from Day 10 onwards. Overall, these results indicated that PTT was able to induce antitumor effects up to Day 5 post-irradiation.

Next, we investigated the tumor tissue and characterized the protein expression. As shown in Fig. 7A and B, HSP70 was significantly upregulated in the PTT-treated tumors on Day 2

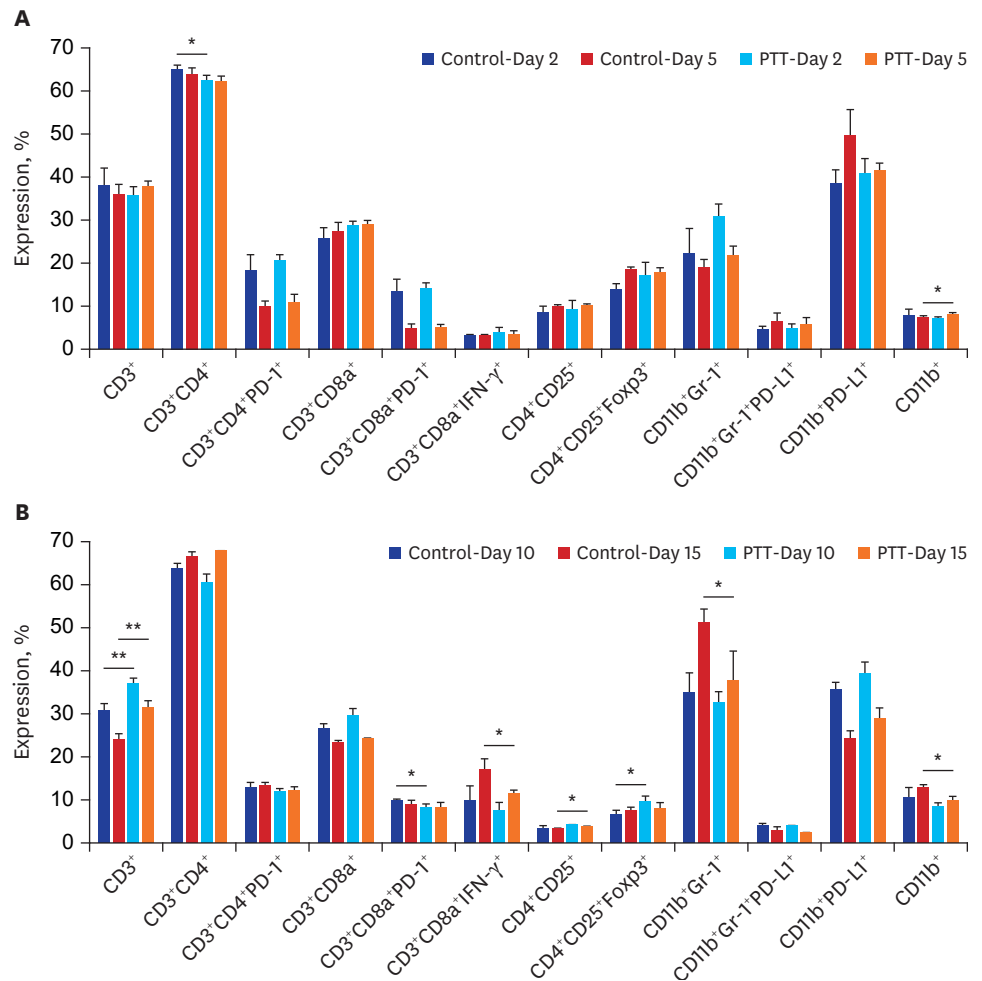


Fig. 5. Immunotolerance activated in spleen after PTT. Quantification of flow cytometric analysis from the spleens of control- and PTT-treated mice on (A) Day 2, Day 5, (B) Day 10, and Day 15 after treatment. Statistical significance was calculated by Student's *t*-test and indicated by **P* < 0.05 or ***P* < 0.01. PTT = photothermal therapy.

and Day 5 compared with the control. Furthermore, HSP70 levels were found to be similar on Day 10 and Day 15, which was indicative of disease progression. As shown in Fig. 7A and C, programmed death-ligand 1 (PD-L1) expression was negligible up to Day 5 after PTT, and increased until Day 15, which indicated that the immunosuppression developed after laser irradiation. Indoleamine 2,3-dioxygenase (IDO) expression was initially suppressed in PTT-treated mice, subsequently upregulated, and similar to the control samples on Day 15 (Fig. 7A and D). As shown in Fig. 7A, E and F, it was also observed that TGF-β and IL-6 expression was upregulated in the tumor tissues of PTT-treated mice from Day 10 post-irradiation. However, ELISA of TGF-β and IL-6 in serum did not show significant changes (Fig. 8A and B).

Subsequently, the tumor tissues isolated from the control- and PTT-treated mice were analyzed by hematoxylin and eosin (H&E) staining to investigate the tissue damage induced by laser irradiation. As shown in Fig. 8C, the tumor section in the control group increased continuously with no obvious tissue damage or necrosis. In contrast, massive necrosis was observed in the PTT treated tumor tissue section on Day 2, and the tumor margin beyond the

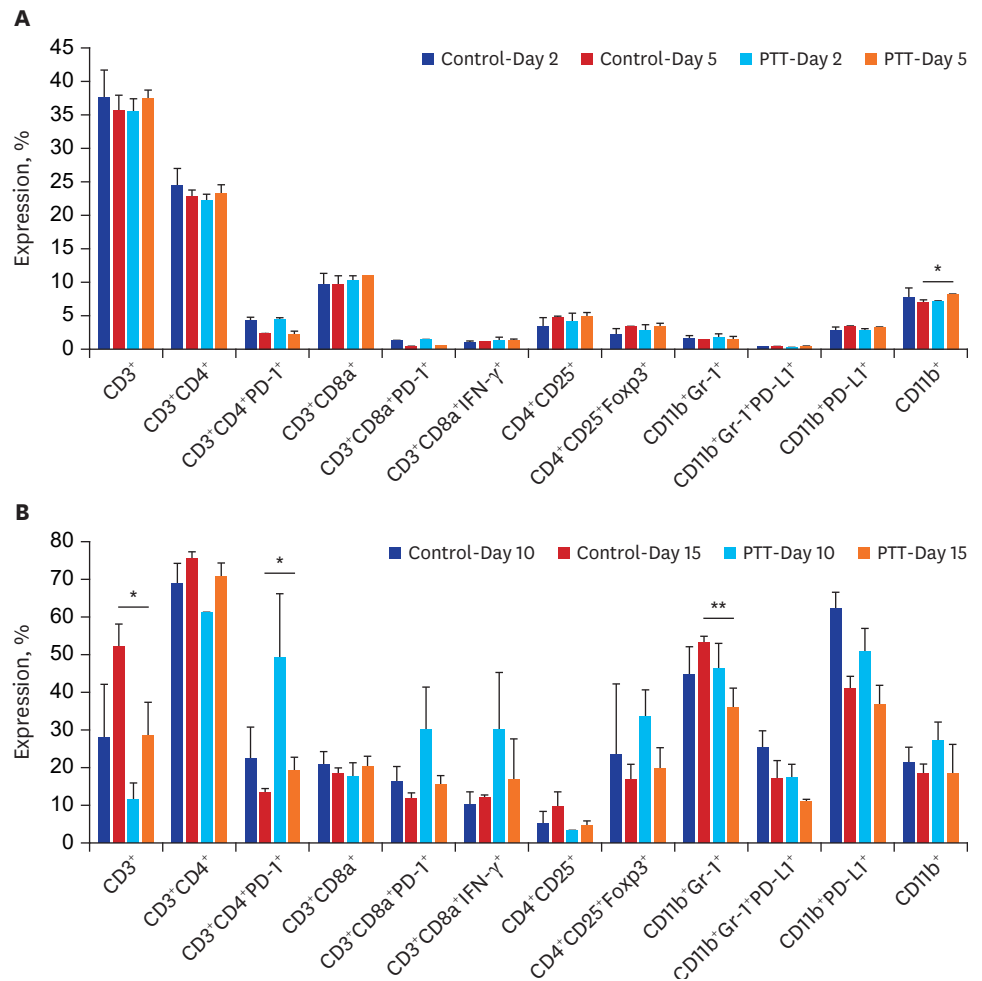


Fig. 6. Immunotolerance activated in peripheral blood after PTT. Quantification of flow cytometric analysis from peripheral blood collected from control- and PTT-treated mice on (A) Day 2, Day 5, (B) Day 10, and Day 15 post-treatment. Statistical significance was calculated by Student's *t*-test and indicated by **P* < 0.05 or ***P* < 0.01. PTT = photothermal therapy.

effective PTT area underwent tumor recurrence from Day 5 onwards (indicated by #). Tumor recurrence around the laser irradiated region (indicated by ^) increased grown in a time-dependent manner up to Day 15.

DISCUSSION

The synthesized liposomes were around 100 nm bearing negative surface charge. PEG-liposomes between 100 and 200 nm in size and with a negative zeta potential possess superior physicochemical properties, such as enhanced systemic circulation and low phagocytic uptake by the reticuloendothelial system.¹⁹ In addition, the optimal surface charge of NPs extends the lifetime and tumor penetration.²⁰ Liposomes also served as efficient carriers for PTT, as ICG encapsulation into liposomes did not alter the heat elevation capabilities of ICG.

The biodistribution studies in a subcutaneous colon cancer model revealed that Lipo-ICG was able to home to tumor within 24 hours of injection. In addition to the EPR effect with

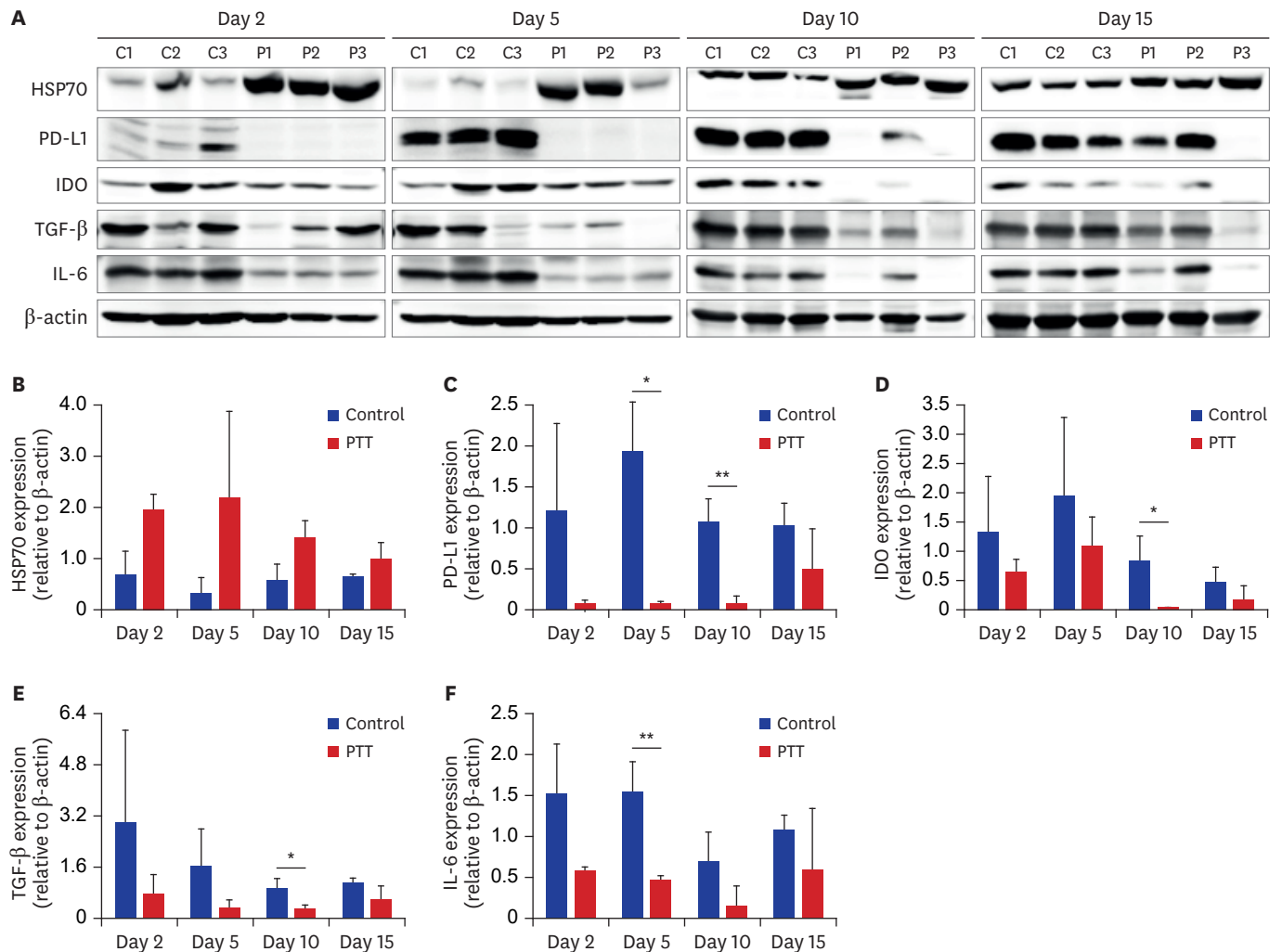


Fig. 7. Evaluation of immunosuppression in the TME. **(A)** Western blotting analysis of tumors isolated from control- and PTT-treated mice on Day 2, Day 5, Day 10, and Day 15 post-irradiation. Control: C1, C2, C3; PTT: P1, P2, P3. Quantification of relative levels of **(B)** HSP70, **(C)** PD-L1, **(D)** IDO **(E)** TGF- β , and **(F)** IL-6 from the blot. Statistical significance was calculated by Student's *t*-test and indicated by **P* < 0.05 or ***P* < 0.01.

HSP = heat shock protein, PD-L1 = programmed death ligand 1, IDO = indoleamine dioxygenase, TGF- β = tumor growth factor- β , IL-6 = interleukin-6, TME = tumor microenvironment, PTT = photothermal therapy.

liposomes, colon cancer is characterized by high leakiness, which contributes to enhanced accumulation in the tumor region.²¹ Also, Lipo-ICG accumulated in the tumor region was able to show elevation in the tumor temperature upon laser irradiation. This result indicated that Lipo-ICG could respond to the external laser irradiation, and generate sufficient heat to kill the tumor cells.

The PTT efficacy was limited to 7 days, and the tumor recurrence rate was increased thereafter. This phenomenon of accelerated tumor regrowth at the tumor margin after PTT was also observed in a recent study.¹² The flow cytometry analysis of spleen and peripheral blood samples indicated that there was a gradual increase in the immunosuppression factors after day 5 post PTT. Also, TGF- β and IL-6 upregulation in the tumor was able to stimulate tumor cell invasion and suppress immune surveillance.²² Many cytokines, such as TGF- β , IDO, and IL-6, which were initially performing normal cellular functions, were transformed after PTT to promote the pro-tumorigenic signaling pathways to create immune evasion and tumor regrowth.

The TME in the peri-tumor region becomes immune tolerant, as characterized by the increased levels of immunosuppressive markers post PTT. In addition, this immune tolerance exhibited after PTT is responsible for the tumor recurrence, compared with the control tumor-bearing mice. The peri-tumor region in which mild heating occurs is mainly involved in the development of the immune tolerant microenvironment.¹² For instance, HSP-70, PDL-1 and IDO in the tumor tissue were found to be upregulated. PTT causes tumor cells to undergo a compensatory stage, wherein HSP70 levels are upregulated to protect the cells from laser-induced thermal damage.²¹ Similarly, the immune evasion properties associated with PD-L1 upregulation in tumor cells has a critical role in the downregulation of the T cell response to tumor cells.²³ IDO enhancement also played a role as an immunomodulatory agent in the regulation of T lymphocyte activity, thereby producing immunotolerance.²⁴ Thus, these results indicated that PTT treatment was ineffective after Day 5, with tumor recurrence in the tumor margin caused by the immunosuppressive microenvironment created after laser irradiation.

In this study, we utilized Lipo-ICG as the therapeutic carrier in combination with PTT and investigated the changes in the tumor microenvironmental that were responsible for the development of immunotolerance. We observed that the effectiveness of PTT for the

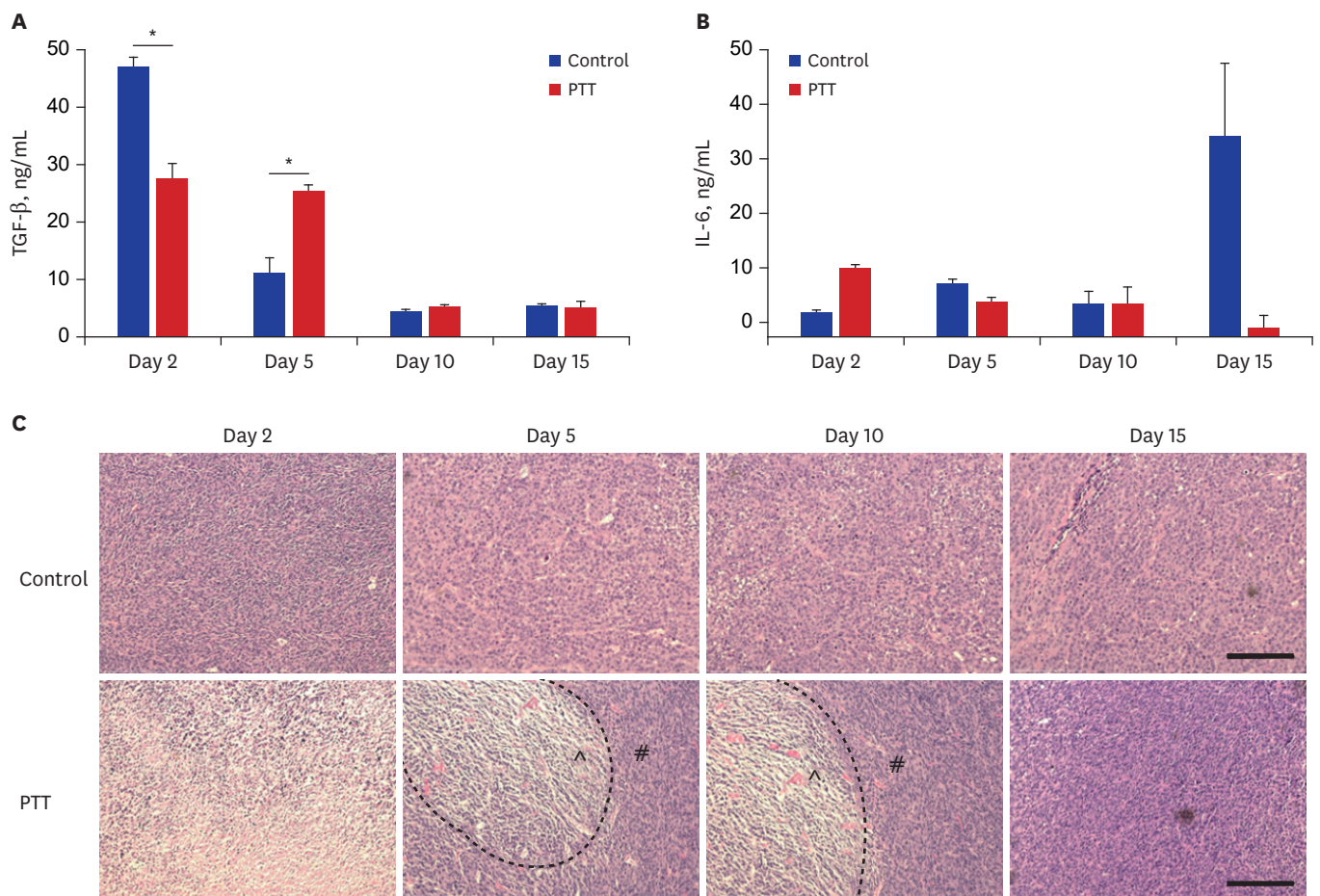


Fig. 8. Immunotolerance & histological analysis. Enzyme-linked immunosorbent assay analysis of serum from control- and PTT-treated mice tested for TGF- β (A) and IL-6 (B). (C) Hematoxylin and eosin assay of tumor tissues. Statistical significance was calculated by Student's *t*-test and indicated by * $P < 0.05$. The ^ symbol indicates the laser irradiated area and the # symbol indicates tumor regrowth. Scale bar = 200 μ m. TGF- β = tumor growth factor- β , PTT = photothermal therapy, IL-6 = interleukin-6.

restriction of the tumor volume was limited to 5 days. The tumor margin beyond the effective PTT depth underwent tumor recurrence more readily than the untreated controls, owing to the upregulation of HSP70, PD-L1, MDSC, T_{reg} s, and similar factors. To efficiently inhibit tumor recurrence, and stimulate the host immune system against cancer, we have identified the inhibitors and suppressors of these potential therapeutic targets, which can be combined with PTT to achieve superior antitumor efficacy with no tumor recurrence.

SUPPLEMENTARY MATERIALS

Supplementary Table 1

Physicochemical characterization of nanoparticles

[Click here to view](#)

Supplementary Table 2

Splenocytes FACS analysis

[Click here to view](#)

Supplementary Table 3

Peripheral blood FACS analysis

[Click here to view](#)

Supplementary Fig. 1

Temperature elevation graph of nanoparticles after laser irradiation (808 nm, 2W/cm², 15 min).

[Click here to view](#)

REFERENCES

1. Zhou M, Zhao J, Tian M, Song S, Zhang R, Gupta S, et al. Radio-photothermal therapy mediated by a single compartment nanoplatform depletes tumor initiating cells and reduces lung metastasis in the orthotopic 4T1 breast tumor model. *Nanoscale* 2015;7(46):19438-47.
[PUBMED](#) | [CROSSREF](#)
2. Wolinsky JB, Colson YL, Grinstaff MW. Local drug delivery strategies for cancer treatment: gels, nanoparticles, polymeric films, rods, and wafers. *J Control Release* 2012;159(1):14-26.
[PUBMED](#) | [CROSSREF](#)
3. Formenti SC, Demaria S. Combining radiotherapy and cancer immunotherapy: a paradigm shift. *J Natl Cancer Inst* 2013;105(4):256-65.
[PUBMED](#) | [CROSSREF](#)
4. Cherukula K, Manickavasagam Lekshmi K, Uthaman S, Cho K, Cho CS, Park IK. Multifunctional inorganic nanoparticles: recent progress in thermal therapy and imaging. *Nanomaterials (Basel)* 2016;6(4):E76.
[PUBMED](#) | [CROSSREF](#)
5. Melamed JR, Edelstein RS, Day ES. Elucidating the fundamental mechanisms of cell death triggered by photothermal therapy. *ACS Nano* 2015;9(1):6-11.
[PUBMED](#) | [CROSSREF](#)
6. Grivennikov SI, Greten FR, Karin M. Immunity, inflammation, and cancer. *Cell* 2010;140(6):883-99.
[PUBMED](#) | [CROSSREF](#)

7. Dong Q, Wang X, Hu X, Xiao L, Zhang L, Song L, et al. Simultaneous application of photothermal therapy and an anti-inflammatory prodrug using pyrene-aspirin-loaded gold nanorod graphitic nanocapsules. *Angew Chem Int Ed Engl* 2018;57(1):177-81.
[PUBMED](#) | [CROSSREF](#)
8. Aggarwal BB, Vijayalekshmi RV, Sung B. Targeting inflammatory pathways for prevention and therapy of cancer: short-term friend, long-term foe. *Clin Cancer Res* 2009;15(2):425-30.
[PUBMED](#) | [CROSSREF](#)
9. Smyth MJ, Dunn GP, Schreiber RD. Cancer immunosurveillance and immunoediting: the roles of immunity in suppressing tumor development and shaping tumor immunogenicity. *Adv Immunol* 2006;90:1-50.
[PUBMED](#) | [CROSSREF](#)
10. Kaur P, Asea A. Radiation-induced effects and the immune system in cancer. *Front Oncol* 2012;2:191.
[PUBMED](#) | [CROSSREF](#)
11. Lin WW, Karin M. A cytokine-mediated link between innate immunity, inflammation, and cancer. *J Clin Invest* 2007;117(5):1175-83.
[PUBMED](#) | [CROSSREF](#)
12. Peng J, Xiao Y, Li W, Yang Q, Tan L, Jia Y, et al. Photosensitizer micelles together with IDO inhibitor enhance cancer photothermal therapy and immunotherapy. *Adv Sci (Weinh)* 2018;5(5):1700891.
[PUBMED](#) | [CROSSREF](#)
13. Bozzuto G, Molinari A. Liposomes as nanomedical devices. *Int J Nanomedicine* 2015;10:975-99.
[PUBMED](#) | [CROSSREF](#)
14. Luo L, Bian Y, Liu Y, Zhang X, Wang M, Xing S, et al. Combined near infrared photothermal therapy and chemotherapy using gold nanoshells coated liposomes to enhance antitumor effect. *Small* 2016;12(30):4103-12.
[PUBMED](#) | [CROSSREF](#)
15. Li AH, Wang Y, Chen T, Zhao W, Zhang AT, Feng SY, et al. NIR-laser switched ICG/DOX loaded thermo-responsive polymeric capsule for chemo-photothermal targeted therapy. *Eur Polym J* 2017;92:51-60.
[CROSSREF](#)
16. Ocoy I, Isiklan N, Cansiz S, Özdemir N, Tan W. ICG-Conjugated magnetic graphene oxide for dual photothermal and photodynamic therapy. *RSC Advances* 2016;6(36):30285-92.
[PUBMED](#) | [CROSSREF](#)
17. Zhang H. Thin-film hydration followed by extrusion method for liposome preparation. *Methods Mol Biol* 2017;1522:17-22.
[PUBMED](#) | [CROSSREF](#)
18. Mojic M, Takeda K, Hayakawa Y. The dark side of IFN- γ : its role in promoting cancer immunoevasion. *Int J Mol Sci* 2017;19(1):E89.
[PUBMED](#) | [CROSSREF](#)
19. Dawidczyk CM, Russell LM, Hultz M, Searson PC. Tumor accumulation of liposomal doxorubicin in three murine models: optimizing delivery efficiency. *Nanomedicine (Lond)* 2017;13(5):1637-44.
[PUBMED](#) | [CROSSREF](#)
20. Blanco E, Shen H, Ferrari M. Principles of nanoparticle design for overcoming biological barriers to drug delivery. *Nat Biotechnol* 2015;33(9):941-51.
[PUBMED](#) | [CROSSREF](#)
21. Yang L, Tseng YT, Suo G, Chen L, Yu J, Chiu WJ, et al. Photothermal therapeutic response of cancer cells to aptamer-gold nanoparticle-hybridized graphene oxide under NIR illumination. *ACS Appl Mater Interfaces* 2015;7(9):5097-106.
[PUBMED](#) | [CROSSREF](#)
22. Jakowlew SB. Transforming growth factor-beta in cancer and metastasis. *Cancer Metastasis Rev* 2006;25(3):435-57.
[PUBMED](#) | [CROSSREF](#)
23. Juneja VR, McGuire KA, Manguso RT, LaFleur MW, Collins N, Haining WN, et al. PD-L1 on tumor cells is sufficient for immune evasion in immunogenic tumors and inhibits CD8 T cell cytotoxicity. *J Exp Med* 2017;214(4):895-904.
[PUBMED](#) | [CROSSREF](#)
24. Munn DH, Mellor AL. Indoleamine 2,3 dioxygenase and metabolic control of immune responses. *Trends Immunol* 2013;34(3):137-43.
[PUBMED](#) | [CROSSREF](#)